

# Mission planning for photogrammetry-based autonomous 3D Mapping of Dams using a commercial UAV

Paulo V. G. Simplicio and Guilherme A. S. Pereira

**Abstract**—The application of autonomous unmanned aerial vehicles (UAVs) for conducting inspections of dams represents an innovative approach aimed at enhancing safety, efficiency, and cost-effectiveness. In this context, this paper presents algorithms for UAV mission design in autonomous dam inspections that include the creation of a 3D map based on photogrammetry. The algorithms were systematically developed to incorporate a comprehensive set of parameters that account for the geometric characteristics of the dam and adhere to photogrammetry specifications. To validate the proposed methodology, we utilized a commercial programmable quadrotor, specifically the Parrot Anafi USA Gov drone, which is equipped with high-quality cameras and can be programmed with the help of a software development kit (SDK) provided by the manufacturer. Our results demonstrate the efficacy of our method, highlighting how the generated maps can be used for hazard detection in the downstream slope of dams.

## I. INTRODUCTION

The advances in technology in the past decades have significantly contributed to the safety of civil infrastructures, such as buildings, bridges, and dams, by providing several techniques and tools, including robots and drones, that are being applied to inspect and prevent catastrophic failures of these structures [1], [2]. This paper presents a methodology for the efficient creation of two-dimensional (2D) and three-dimensional (3D) maps of dams using UAVs. The method was tested in an actual water dam, as shown in Fig. 1, generating high-resolution maps that eventually will be used for frequent and low-cost inspections of the dam. A video summarizing our experiments can be watched here: <https://youtu.be/SuqJXi0uRdk>.

As highlighted in [3], accidents involving dams, especially the large tailing dams associated with mining, can be catastrophic and result in the deaths of thousands of people. In the United States, the average age of dams is 65 years old, while 50 years is considered the reasonable safety limit [4]. Cracking, seepage, and overtopping are among the main reasons for dam failures, particularly due to the lack of inspections and proper maintenance [5]. Since the embankment of most dams is made with cheaper and weaker materials, like soil and stones, rather than concrete, correct and frequent inspections are strongly necessary to prevent seepage, cracks, and further collapse [6]. In recent years, the

This work was supported by the Department of Energy of the United States of America (DOE), Grant DE-FE0032206.

Paulo V. G. Simplicio and Guilherme A. S. Pereira are with the Department of Mechanical, Materials and Aerospace Engineering, Benjamin M. Statler College of Engineering and Mineral Resources, West Virginia University, Morgantown, WV, 26501, USA. Emails: [pvg00001@mix.wvu.edu](mailto:pvg00001@mix.wvu.edu), [guilherme.pereira@mail.wvu.edu](mailto:guilherme.pereira@mail.wvu.edu)



Fig. 1. Downstream slope of the Upper Deckers Creek dam (WV, U.S.A.), the Parrot Anafi USA Gov drone used in the experiments of this paper, and an example of a dam inspection trajectory specified using the requirements of the mission.

growing use of mobile, marine, and aerial robots to aid the inspection of dams is notable [7]–[11].

Regarding the application of robots for dam inspections, the authors of [7] developed a method to inspect the slope of a dam using a remotely operated vehicle (ROV). The proposed vehicle is equipped with acoustic and optical sensors and can correct its trajectory using onboard GPS. In [8], a low-cost autonomous underwater vehicle (AUV) was developed for the inspection of dams. The goal was to create a low-cost device capable of providing information about the siltation level (concentration of silt or clay in water) and inspecting the dam wall.

Aiming to perform a complete inspection of a dam in a short amount of time, the use of aerial vehicles such as quadrotors has increased in the past few years. In [10], a UAV running the YOLO algorithm was applied to quickly detect cracks in a dam. In the same line, [11] shows a solution based on the use of two deep neural networks for object detection, specifically a Faster R-RCNN and a Single Shot Multibox Detector. Similarly, we can find different projects in the literature that work only with images for hazard detection, instead of three-dimensional (3D) point clouds. One of the main disadvantages of using images is that they only provide a two-dimensional (2D) representation of the scene, lacking detailed depth information. As an alternative that still uses images, photogrammetry techniques can generate

dense 3D point clouds with a large number of points without the need for light detection and ranging (LiDAR) sensors, enabling a more detailed representation of the dam. This is particularly valuable for applications requiring fine details or precise measurements that rely on comparisons over time, considering different weather conditions.

In summary, photogrammetry is a technique used to generate 3D models of structures and objects through a series of images. Currently, photogrammetry has been employed in several fields, such as civil construction, agriculture, geology, and engineering. One of the significant advantages is the capability to generate point clouds and high-resolution 3D maps solely with images, without the need for LiDARs. However, to achieve excellent 3D reconstruction of a structure, it is necessary to consider specific factors, including image resolution, overlap between two consecutive images, and distance to the object [12].

The main goal of the project in which this paper is inserted is to help prevent dam accidents by developing an autonomous aerial system for the inspection and monitoring of active and abandoned dams using photogrammetry. Despite the existence of methodologies for path and mission planning of drones performing photogrammetry-based 3D mapping in the literature, except for a few papers like [13], [14], its accessibility may be hindered by fragmentation across various sources. To overcome this, this paper consolidates and synthesizes this dispersed methodology into a comprehensive document, enhancing the mission planning methodology for 3D mapping of dams and considering parameters usually neglected, such as the slope of the structure. We have meticulously tailored the methodology to effectively tackle the specific challenges of inspecting the sloped areas of a dam with a commercial UAV and also present the lessons learned with its application in an actual dam. Although we present experiments focusing on 3D mapping, data collected during the proposed mission can be also used to compose 2D maps (i.e., orthomosaics), which may be useful in some applications.

The rest of this paper is organized as follows: Section II presents an overview of photogrammetry, detailing the essential steps involved. Section III provides the methodology proposed for dam inspection. Following that, Section IV presents the results of our practical experiments. This section also contains a discussion about the lessons learned during the execution of our experiments. Finally, Section V concludes the paper and offers perspectives for future works.

## II. PHOTOGRAMMETRY

Photogrammetry is a technique widely employed for generating accurate mappings by extracting three-dimensional information from two-dimensional data [15], [16]. At the core of photogrammetry lie the principles of aerial triangulation and stereoscopy, instrumental for precisely measuring angles, distances, and elevations. In essence, aerial triangulation establishes relationships between images captured from different viewpoints, crucial for determining camera position and orientation, correcting distortions, and creating precise

three-dimensional maps [17]. Stereoscopic vision enhances spatial representation by considering diverse perspectives captured in overlapping images [18].

To initiate the photogrammetric mapping process, specific steps must be followed. The initial step involves acquiring overlapping images to enable accurate feature matching and robust triangulation. This process is essential not only for map generation but also for producing other visual information, such as orthomosaics (several photos stitched together to compose a planar map of a region), utilizing the photogrammetric process [19]. Methodical image acquisition, coupled with the correct definition of parameters like the Ground Sampling Distance (GSD), ensures high-resolution mapping. Here the GSD represents the physical size of one pixel relative to the ground. Additionally, the camera choice (focal length, lens distortions, sensor resolution, etc) and weather conditions (lighting conditions and wind) can collectively impact the overall map quality [20].

The subsequent step of photogrammetry entails camera calibration and orientation, when a photogrammetry software processes the input images, extracting intrinsic camera parameters such as focal length, aspect ratio, and pixel size. Simultaneously, the software determines the position and orientation of each image in the 3D world. Both camera calibration and orientation are critical for the generation of precise 3D maps. At the end of this step, a sparse point cloud is reconstructed, representing three-dimensional coordinates of features on the Earth's surface. This sparse point cloud serves as the foundation for the development of the dense point cloud and the subsequent reconstruction of the 3D map [20].

Additionally, specific parameters for aerial photogrammetry may vary depending on the structure's shape under inspection. For example, if the structure is too large to fit within a single horizontal flight, multiple coverage rows become necessary. Moreover, the shape of the structure plays a crucial role in determining the optimal path. The following section outlines several photogrammetry parameters tailored to our work, including the number of coverage rows, and explains how we use them to plan the mission and define trajectory parameters.

## III. METHODOLOGY

In this section, we outline the methodology used in this paper for UAV-based photogrammetry of dams. Considering the downstream slope of a dam, we address key questions such as the flight proximity to the point of interest, vertical and lateral overlap, GSD, number of coverage lines, and speed of the UAV to achieve an optimal flight result. Moreover, we provide an algorithm that considers the best flight plan based on the object (hazard) size we want to detect. In other words, we create a mission that aims to achieve a sufficient resolution for the size of the hazards we expect to find on the downstream slope of a dam. Taking into consideration the parameters of the camera used in the mission, the developed algorithm takes as an input the size of the object we want to

detect and the image overlap. With this algorithm, we obtain a good balance between accuracy and flight time.

### A. Mission Planning Approach

This subsection describes all the details regarding the mission planning development. To illustrate our methodology, we will consider the Upper Deckers Creek dam presented in Fig. 1, where the experiments of this paper were also conducted. The first step of our approach is to define a simplified shape for the structure we want to inspect. As observed in this dam and many others worldwide, the downstream slope face can be approximated by a trapezoidal shape. For mission planning purposes, we consider an isosceles trapezoid in the Euclidean three-dimensional space. To obtain the dimensions that compose the trapezoid, we may utilize the plan of the dam (CAD file) or perform measurements *in loco*, before we apply a few trigonometric calculations.

After considering the shape of the dam as a trapezoid, we can easily see that a back-and-forth path (also known as lawn-mower or boustrophedon path) (Fig. 1) is the most indicated method to establish a pattern of overlapping images for photogrammetry. Commercial drones can usually use both GPS coordinates and or waypoints relative to an initial position to follow a path. Based on this, we initiate a mission by defining the home and initial positions and storing them as GPS coordinates. In this context, the home position is where the UAV takes off and lands, and the initial position is set as the spot where the drone begins the back-and-forth trajectory (point above the white dot in Fig. 2). After reaching the initial position, we start sending relative waypoints, given as displacements from the initial position.

In order to calculate the path needed for the inspection, it is important to first define the desired GSD based on the hazard size we aim to identify, which will provide the distance to the dam. A lower GSD results in higher map resolution. For instance, if our mission does not require a very high resolution, and we set a GSD of 5 cm/px for our camera parameters, flying 125 m from the downstream slope face would be sufficient to form a single horizontal line trajectory. In this scenario, there is no need to consider parallel paths/coverage rows, and consequently, no need to address the vertical overlap between coverage rows but only the lateral overlap. To achieve the desired lateral overlap, we must control the UAV speed and capture images at defined intervals (see Section III-B). However, for a smaller GSD, essential for a high-resolution map, the drone would need to fly closer to the downstream slope of the dam, resulting in a loss of field of view. In this situation, multiple coverage rows are essential for the back-and-forth trajectory, and we must consider not only the lateral overlap but also the vertical overlap between images taken in different rows.

The generation of the UAV's path considers parameters such as the width of the inspection area, the number of coverage rows, the distance between each line, and the dam-approaching movement based on the slope (necessary to keep a constant distance between the camera and the slope). A list of two waypoints per row is created for the back-and-forth

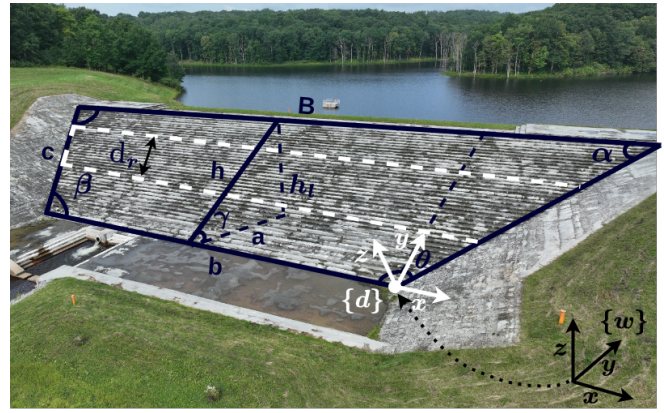


Fig. 2. Defined trapezoid for the downstream slope of the Upper Deckers Creek dam with the followings dimensions: small base (b): 63.5 m, long base (B): 127 m, height (h): 38.5 m, legs (c): 50 m,  $h_1$ : 12.2 m, a: 36 m, and slope ( $\gamma$ ): 19 degrees, Obtuse angle: 129.42 degrees, Acute angle: 50.58 degrees. Both coordinate systems used in our method are also presented:  $\{w\}$ , used by the UAV and  $\{d\}$  where a planar path parallel to the dam is initially created.

path by iteratively extending an ordered set of  $x$ ,  $y$ , and  $z$  coordinates in the world reference frame  $\{w\}$ , where  ${}^w x$  is defined as the axis parallel to the main dimension of the dam,  ${}^w z$  points up, and  ${}^w y$  is defined by the right-hand rule (see the black reference frame in Fig. 2). The origin of reference frame  $\{w\}$  is defined as the lowest right corner of the dam.

To describe how the path is created, we consider a second reference frame,  $\{d\}$ , which origin coincides with the origin of  $\{w\}$ . (Fig. 2). Similar to  $\{w\}$ , frame  $\{d\}$  also has axis  ${}^d x$  parallel to the main dimension of the dam, but  ${}^d y$  is now parallel to the height of the trapezoidal region representing the dam, and  ${}^d z$  is orthogonal to the dam. Initially, we define the list of waypoints in the dam's reference frame  $\{d\}$  and then rotate them to  $\{w\}$ . This simplifies the computation since the waypoint coordinates in the  ${}^d z$  axis will represent the distance to the slope face ( $d_s$ ), which is constant for all coverage rows.

As the waypoints along the  ${}^d y$  axis vary for each row, it becomes crucial to account for both the number of coverage rows ( $N$ ) and the distance between them ( $d_r$ ), as detailed in the subsections III-B.3 and III-B.4, respectively. With this information, we calculate the initial  ${}^d y(0)$  as

$${}^d y(0) = \frac{h - (d_r \times (N - 1))}{2}, \quad (1)$$

where  $h$  is the height of the trapezoid, as illustrated in Fig. 2. The waypoint coordinates in the  ${}^d y$  axis for the  $k^{\text{th}}$  row are calculated in function of the coordinate for row 0 as

$${}^d y(k) = {}^d y(0) + k \times d_r, \quad \text{for } k = 1, \dots, N. \quad (2)$$

For the  ${}^d x$  axis, the width of the dam is adjusted for each row by an increment considering angle  $\theta$  as

$$\delta_w(k) = \delta_w(k - 1) + \tan(\theta) \times d_r, \quad (3)$$

where  $\delta_w(0) = 0$  and  $\theta = \beta - 90^\circ$ . In fact,  $\delta_w(k)$  represents half of the increment of each row since it is

---

**Algorithm 1** Waypoints Generation
 

---

```

1: Input:  $N, d_s, d_r, h, w_d, \theta, \gamma$ 
2: Output:  $w_\tau$  (ordered set of waypoints  $w_x, w_y, w_z$ )
3:  $\delta_w(0) \leftarrow 0$ 
4:  $d_x(0) \leftarrow 0$ 
5:  $d_y(0) \leftarrow \frac{h - (d_r \times (N-1))}{2}$ 
6:  $d_z(0) \leftarrow d_s$ 
7:  $X \leftarrow d_x(0), Y \leftarrow d_y(0), Z \leftarrow d_z(0)$ 
8: For  $k$  from 0 to  $N$  do
9:   if  $k$  is even:
10:     $X \leftarrow X \cup [(d_x(0) + \delta(k)), (d_x(0) - w_d - \delta(k))]$ 
11:   else:
12:     $X \leftarrow X \cup [(d_x(0) - w_d - \delta(k)), (d_x(0) + \delta(k))]$ 
13:     $Y \leftarrow Y \cup [d_y(0) + k \times d_r, d_y(0) + k \times d_r]$ 
14:     $Z \leftarrow Z \cup [d_z(0), d_z(0)]$ 
15:     $\delta_w(k+1) \leftarrow \delta_w(k) + \tan(\theta) \times d_r$ 
16: End For
17:  $w_\tau \leftarrow rot_{x,\gamma}([X, Y, Z])$ 
18: Return  $w_\tau$ 

```

---

used to change the  $x$  coordinates of the two waypoints in row  $k$  with respect to row  $k-1$  to match the leg of the trapezoid. The  $x$  coordinates of the  $k^{\text{th}}$  row are then defined as  $d_x = d_x(0) + \delta(k)$  and  $d_x = d_x(0) - w_d - \delta(k)$ , where  $w_d$  is the short base of the trapezoid. Algorithm 1 summarizes the computation of the complete path. In this algorithm,  $d_x(0) = 0$ ,  $d_y(0)$  is calculated as in (1), and  $d_z(0) = d_s$ .

As seen in the Algorithm 1, at each step, we generate waypoints for  $d_x$ ,  $d_y$ , and  $d_z$  axis to create the path for each row. Note that, for the  $d_x$  axis, we generate two waypoints for each row, considering the start and end point. However,  $d_y$  and  $d_z$  remain constant for each row since we only move forward or increase altitude when moving to the next row.

To account for the slope angle of the dam ( $\gamma$ ), we perform a rotation around the  $x$ -axis, transforming from the dam frame to the world frame. This is done by multiplying each waypoint ( $d_x, d_y, d_z$ ) by a rotation matrix as:

$$\begin{bmatrix} w_x(k) \\ w_y(k) \\ w_z(k) \end{bmatrix} = \begin{bmatrix} 1 & 0 & 0 \\ 0 & \cos(\gamma) & -\sin(\gamma) \\ 0 & \sin(\gamma) & \cos(\gamma) \end{bmatrix} \begin{bmatrix} d_x(k) \\ d_y(k) \\ d_z(k) \end{bmatrix}. \quad (4)$$

### B. Trajectory Parameters

This subsection details how the parameters of the trajectory are defined in the previous section considering the photogrammetry parameters and the dam shape. This methodology encompasses some of the methods presented in [21] and [22].

1) *Flight Proximity to the point of interest:* To determine how close the drone should fly to the point of interest (downstream slope of the dam, in this case), we need to calculate the distance from the camera to the slope face ( $d_s$ ). Distance  $d_s$  can be calculated based on the desired GSD value, focal length ( $F_L$ ), number of pixels width ( $P_N$ ), and sensor width ( $S_W$ ) as:

$$d_s = \text{GSD} \times F_L \times \frac{P_N}{S_W \times 100}, \quad (5)$$

Given the parameters of the camera, the key variable in (5) is the GSD, which is based on the object size we want to identify. According to Teledyne Lumenera, 2023 [23], the GSD should be defined as at least half of the smallest dimension of the object we want to detect. We also consider that, for a good reconstruction, the GSD size should be no higher than 2.5 cm/px. In this regard, even when the size of the smallest object is larger than 5 cm, the GSD will be set as 2.5 cm/px.

2) *Camera Footprint:* The camera footprint ( $L$ ) represents the area covered by the camera's field of view when mounted on the UAV. We can calculate  $L$  using:

$$L = 2d_s \times \tan\left(\frac{\text{FOV}}{2}\right), \quad (6)$$

where  $d_s$  is the distance from the slope face and FOV is the field of view that can be either vertical or horizontal. We use the VFOV to calculate the vertical overlap of images and the HFOV to calculate the lateral overlap.

3) *Number of Coverage Rows:* The number of coverage Rows ( $N$ ) can be determined based on the desired vertical overlap between two images ( $S_v$ ) and the height of the coverage area ( $h$ ) as:

$$N = \frac{h}{L \times (1 - S_v)}, \quad (7)$$

where  $S_v$  is within the range 0 to 1, representing an overlap from 0% to 100%. According to [24], the recommended minimum vertical overlap is 50% with a minimum lateral overlap of 20% for a feasible photogrammetry. However, it is advisable to aim for a vertical overlap of at least 70% and a lateral overlap of at least 60% for the best results.

4) *Distance Between Coverage Rows:* To determine the distance between coverage rows ( $d_r$ ), we divide the height of the coverage area ( $h$ ) by the number of coverage lines ( $N$ ):

$$d_r = \frac{h}{N}. \quad (8)$$

5) *Lateral Speed:* The lateral speed can be calculated based on the desired lateral overlap ( $S_l$ ), camera footprint ( $L$ ), and frame rate in frames per second ( $f$ ) as:

$$\text{Speed} = \frac{1 - S_l}{L \times f}. \quad (9)$$

### C. Numerical Example

The process to determine a flight plan for the UAV in a dam inspection task is summarized in Algorithm 2. By using this algorithm, the camera parameters for the Parrot Anafi USA Gov drone used in our experiments (Table I), the desired overlaps, and the required GSD, we can calculate the distance from the slope face ( $d_s$ ) and other relevant parameters. For example, if we consider that the smallest dimension of the smallest object we want to identify is 2.25 cm, the GSD could be specified as  $2.25/2 = 1.125$  cm/px. With the downstream slope of the dam presented in Fig. 2 and vertical and lateral overlaps of 80%, we applied the algorithm and obtained the mission parameters outlined in Table II.

## Algorithm 2 Trajectory Parameters Calculation

- 1: **Input:** Object Size,  $F_L$ ,  $P_N$ ,  $S_W$ ,  $S_v$ ,  $S_l$ ,  $h$ ,  $s$ ,  $f$
- 2: **Output:**  $d_s$ ,  $L$ ,  $N$ ,  $d_r$ , Speed
- 3: **Step 1:** Calculate  $GSD$
- 4:  $GSD \leftarrow$  Object Size/2
- 5: **Step 2:** Calculate  $d_s$
- 6:  $d_s \leftarrow GSD \times F_L \times \frac{P_N}{S_W \times 100}$
- 7: **Step 3:** Calculate  $L$
- 8:  $L \leftarrow 2d_s \times \tan\left(\frac{FOV}{2}\right)$
- 9: **Step 4:** Calculate  $N$
- 10:  $N \leftarrow \frac{h}{L \times (1 - Ov)}$
- 11: **Step 5:** Calculate  $d_r$
- 12:  $d_r \leftarrow \frac{h}{N}$
- 13: **Step 6:** Calculate speed
- 14: Speed  $\leftarrow \frac{1 - S_l}{L \times f}$
- 15: **Return**  $d_s$ ,  $L$ ,  $N$ ,  $d_r$ , Speed

TABLE I

PARROT ANAFI USA GOV CAMERA PARAMETERS

Parameter	Value
Focal Length ( $F_L$ )	4 mm
Sensor Diagonal ( $S_D$ )	7.487 mm
Sensor Width ( $S_W$ )	6.140 mm
Sensor Height ( $S_H$ )	5.497 mm
Number of Pixels ( $P_N$ )	3840
Horizontal Field of View (HFOV)	84°
Vertical Field of View (VFOV)	69°

Fig. 3 presents an example of the optimal trajectory calculated with the developed algorithm. The red trapezoid represents the downstream slope of the dam and the blue lines represent the path with the waypoint coordinates ( $x$ ,  $y$ , and  $z$ ) evidenced. To make sure that the camera is oriented towards the downstream slope of the dam while the UAV is following the path, its gimbal has to be adjusted to match the slope of the dam ( $\gamma$ ). For our experiments described in the next section, the tilt angle was set to  $-71$  degrees ( $-90^\circ + \gamma$ ), where  $-90$  degrees correspond to the tilt gimbal angle that is orthogonal to the  ${}^w y$ -axis.

## IV. EXPERIMENTS

This section presents our experiments, including information related to the software used for the 3D mapping. The section also presents some lessons learned during the development of this work.

### A. Experimental Setup

The Parrot Anafi USA Gov was selected as the quadrotor for this work, primarily for being a high-end drone specifically designed for the U.S., where it is compliant with the National Defense Authorization Act (NDAA) and the Trade Agreements Act (TAA), and is approved under the Blue sUAS program [25]. The aircraft has two RGB sensors of 1/2.4": a wide photo sensor with a resolution of 21 MP and a Field of View (FOV) of 84°; and a rectilinear sensor of 16 MP resolution with an FOV of 75.5°. The parameters of

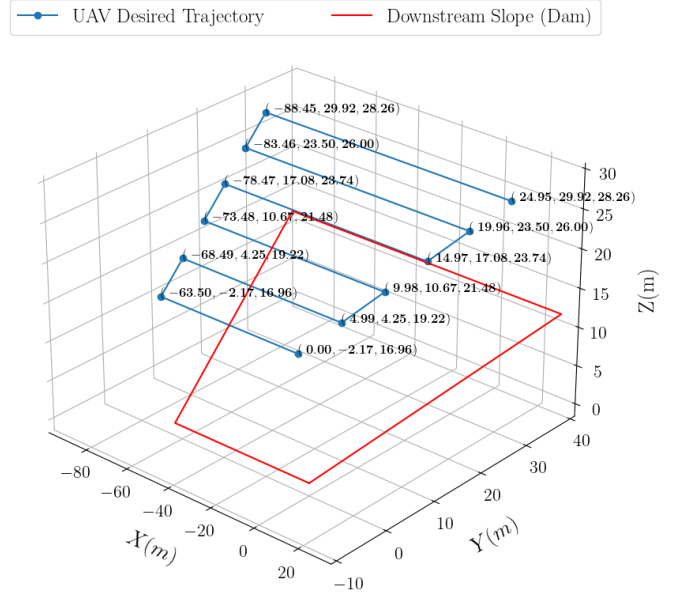


Fig. 3. The coverage rows forming the optimal path when we have a GSD of 1.125 cm/px, a distance to the dam of 27.93 m, and an overlap of 80%.

the wide camera used in our experiments are summarized in Table I.

TABLE II

FLIGHT PLAN SUMMARY

Parameter	Value
Distance to the slope face ( $d_s$ )	27.93 m
Number of coverage lines ( $N$ )	6
Distance between coverage rows ( $d_r$ )	6.42 m
Ground Sampling Distance (GSD)	1.125 cm/px

It is worth noting that, although the HFOV is given by the camera manufacturer, the VFOV in Table I was calculated based on the  $S_H$  as:

$$VFOV = 2 \times \arctan\left(\frac{S_H}{2 \times F_L}\right). \quad (10)$$

Besides the advanced hardware specifications [26], the Anafi USA Gov can easily be programmed and controlled by a computer through the Olympe [27] SDK interface. This interface facilitates communication between the drone and a Linux-based computer. Inspired by [28], in our project, we developed our own version of an Olympe wrapper for the Robot Operating System 2 (ROS 2) [29], which facilitates data collection and integration with other robotics software available in ROS 2.

To investigate the methodology in a real environment, we conducted experiments above the downstream slope of the Upper Deckers Creek dam in West Virginia. Fig. 1 depicts the test environment along an example of a dam inspection mission. The objective was to execute a trajectory based on selected parameters, aiming for a balance between resolution and flight time. The GSD was varied and defined considering the size of the hazards we aimed to identify.



Fig. 4. 3D map of the downstream slope of the Upper Deckers Creek Dam, with a two-coverage rows mission (GSD: 1.40 cm/px).

Besides 3D point clouds of the unaltered dam, we also created a point cloud of the downstream slope containing simulated hazards and checked our ability to identify them within the point cloud. For this task, we added a box (dimensions  $53 \times 36 \times 30$  cm) and two soccer balls (21 cm in diameter) to the slope face of the dam, thus mimicking hazards of different sizes. We then verified the effectiveness of the methodology applied by first defining the GSD based on half the size of the smallest object we aimed to identify.

Since the smallest object in our study is a soccer ball, resulting in a GSD of 10.5 cm, the photogrammetric map’s resolution would be low, with a flight distance to the wall of 262.67 m. This distance is impractical, considering that the Federal Aviation Administration’s (FAA) maximum height allowance of 120 m in the United States. To address this, we explored smaller GSD values to achieve a higher resolution while maintaining a reasonable flight height. Table III presents various GSD values used in our missions.

### B. COLMAP and CloudCompare

To generate and analyze the point clouds and 3D maps of the dam, we used two open-source software applications: COLMAP [30], [31] and CloudCompare<sup>1</sup>. COLMAP is a general-purpose Structure-from-Motion (SfM) and Multi-View Stereo (MVS) pipeline that generates a point cloud in two major steps: feature detection and feature extraction, and structure and motion reconstruction. The software uses the images to generate a sparse point cloud first and then a

<sup>1</sup><https://www.danielgm.net/cc/>

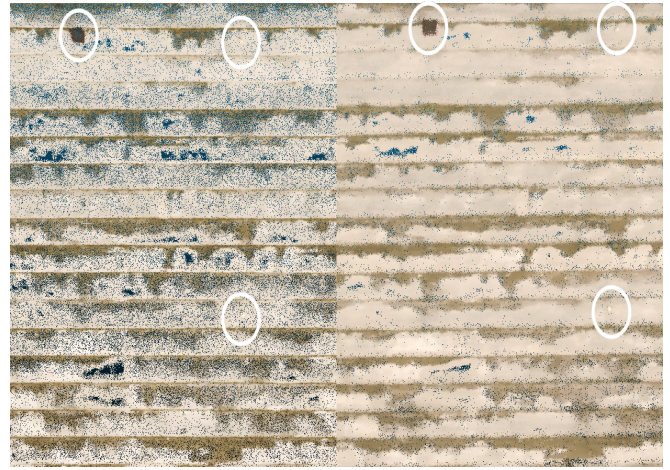


Fig. 5. Hazard simulation results: long-range mission (left) and detailed mission (right).

dense point cloud. After that, we can import and visualize the dense point cloud using COLMAP. However, visualizing the dense mesh, which consists of vertices, edges, and faces, requires an external viewer such as CloudCompare. This is a 3D point cloud processing software able to open point clouds and meshes and perform comparisons between two dense 3D point clouds.

### C. Results

In our effort to analyze the proposed method for dam inspections, we conducted four sets of experiments using different missions, as outlined in Table III. The first mission was not possible to perform due to the fly height. The second mission, with a GSD of 4.20 cm/px, did not provide sufficient resolution to discern hazards, while the third mission, with a GSD of 2.10 cm/px, yielded results similar to the fourth mission. In this context, we focus our discussion on the fourth and fifth missions, considering a 1.40 cm/px GSD and a longer one aimed at a GSD of 0.84 cm/px. A video summarizing the experiment can be found at <https://youtu.be/SuqJXi0uRdk>.

The first mission was called a long-range mission, aimed to inspect the dam and generate a high-resolution map swiftly. For this case, we used our algorithm to compute the parameters presented in the first column of Table IV. The 3D map generated is shown in Fig. 4. The second mission was a detailed mission, where the UAV flew closer to the slope face of the dam, resulting in a denser point cloud and a higher resolution. The parameters for this mission are presented in

TABLE III  
DISTANCE TO THE SLOPE FACE AND AND NUMBER OF COVERAGE ROWS FOR DIFFERENT GSD VALUES

Mission	Object Size	GSD	Distance to the slope face ( $d_s$ )	Overlap	Rows ( $N$ )
1	21/2 cm	10.50 cm/px	262.67 m	60 %	1
2	21/5 cm	4.20 cm/px	105.07 m	60 %	1
3	21/10 cm	2.10 cm/px	52.53 m	60 %	1
4	21/15 cm	1.40 cm/px	35.02 m	60 %	2
5	21/25 cm	0.84 cm/px	21.01 m	60 %	4

TABLE IV  
MISSION PLAN RESULTS

Parameter	Two Coverage Rows Mission	Four Coverage Rows Mission
Distance to the dam slope ( $d_s$ )	33.52 m	21.01 m
Number of coverage rows ( $N$ )	2	4
Distance between coverage rows ( $d_r$ )	19.250 m	9.625 m
Ground Sampling Distance (GSD)	1.4 cm/px	0.84 cm/px
Number of point cloud points	8,497.049	37,525.105

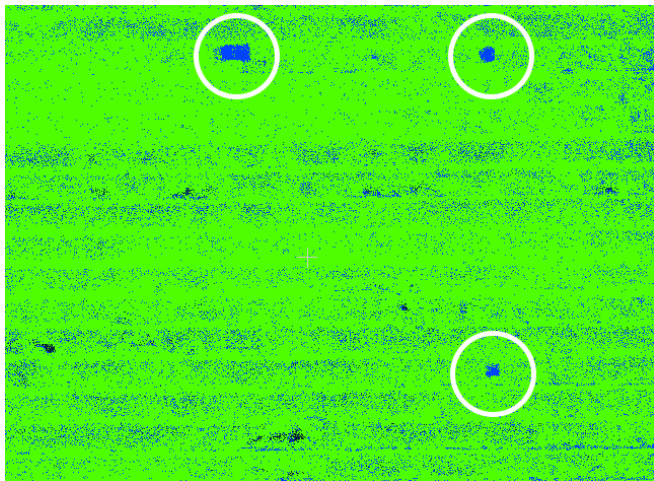


Fig. 6. Hazards identified within point clouds (detailed mission GSD: 1.40 cm/px) after registration and comparison of point clouds with and without simulated hazards.

the second column of Table IV. We can visually observe the density difference between the two point clouds in Fig. 5, and also by the number of points in the last row of Table IV. Despite the significant disparity in the number of points, the long-range mission also exhibited a very high resolution, producing a 3D map similar to the detailed mission but with half the operation time. In Fig. 5 we see that in both cases, we can see the objects simulating hazards (box and two soccer balls) on the point cloud of the slope face of the dam. There is a slight improvement in resolution when a smaller GSD is employed; consequently, hazards become more visible.

In order to automatically detect the simulated hazards, we loaded the point clouds with and without hazards into CloudCompare and performed registration. In this process, we aligned both point clouds and compared the cloud-to-cloud distance. Fig. 6 presents the region of the point clouds that contains the hazards. As can be seen, the hazards are highlighted in blue after the comparison. More processing needs to be done to extract this information from the resultant point cloud.

#### D. Lessons Learned

We now summarize the main lessons learned during the development of this project. The literature of photogrammetry indicates that a good practice is to have a GSD value at least half the size of the smaller object (hazard) you want to identify. However, our practical results showed that, for point cloud reconstruction, half the size of an object is not sufficient for an accurate identification of the hazard in the

resultant point cloud. In our case, a GSD equal to one-tenth of the object's size was identified as effective. This disparity is probably because the current literature only considers GSD as a form of visual identification of objects in an image, but does not consider the needs for a good 3D reconstruction. In the continuation of this research, we expect to define new baselines for the GSD when this is required.

Another important lesson involves the need for a precise adjustment of the camera angle to align with the slope of the dam. In previous experiments using the FreeFlight 6 software provided by the UAV's manufacturer, achieving precise adjustment was challenging because the software allowed only a graphical range input instead of an exact value for the angle. In such cases, for flights with fewer coverage rows, a noticeable lack of density in some parts of the reconstruction was observed.

Finally, a significant aspect is the GPS accuracy. Although GPS was enough to provide good odometry during path following, in certain experiments, during autonomous return to home and landing, a higher error was observed. Although the UAV consistently landed in the vicinity of the landing pad, we are currently implementing an object detection algorithm to identify the landing pad and ensure a centered landing. This implementation will play a crucial role in enhancing operational safety, especially in situations with confined spaces. Vehicles with Real-time kinematic (RTK) positioning may be used to avoid such extra software.

#### V. CONCLUSIONS AND FUTURE WORK

This paper presented a methodology for inspecting dams using commercial UAVs by creating photogrammetry-based point clouds and 3D maps using a UAV. The mission planning approach was defined, considering optimal parameters to achieve good 3D reconstruction in a short amount of time. However, it is important to notice that the same methodology could be used to generate 2D maps, which may be useful for the detection of some specific hazards (e.g., seepage using a thermal camera). Results show that by defining parameters such as the GSD and image overlap, it is possible to successfully create long-range and detailed missions.

Currently, we are simulating hazards on the downstream face of the dam by incorporating objects that mimic cracks and other potential issues that may contribute to failure. The objective is to automatically detect these anomalies in the point clouds and classify them as hazards. Using CloudCompare, we can simply compare the point clouds with previous point clouds to identify any type of anomaly. Future work includes the application of the methodology described in

this paper to inspect tailing dams, which are used to store waste byproducts of mining and are constructed with the same material they store. Recent catastrophic accidents with tailing dams motivate the use of new technologies for their frequent and precise inspections [32]. To completely inspect such dams, the methods proposed here need to be extended to create maps of other important structures, such as emergency spillways, which are long open channels that guide the water and tailings to safe regions in case of accidents.

#### ACKNOWLEDGEMENTS

The authors would like to thank Professor John Quaranta from WVU, and Mr. Davin White from West Virginia Conservation Agency for facilitating our access to and providing the plans for the Upper Deckers Creek dam, where the experiments of this paper were conducted.

#### REFERENCES

- [1] S. U. Rehman, M. Usman, M. H. Y. Toor, and Q. A. Hussaini, "Advancing structural health monitoring: A vibration-based iot approach for remote real-time systems," *Sensors and Actuators A: Physical*, vol. 365, 2024.
- [2] A. Nguyen, V. Gharehbaghi, N. T. Le, L. Sterling, U. I. Chaudhry, and S. Crawford, "Asr crack identification in bridges using deep learning and texture analysis," *Structures*, vol. 50, pp. 494–507, 2023.
- [3] S. American. (2023) Dams worldwide are at risk of catastrophic failure. Accessed January 09, 2024. [Online]. Available: <https://www.scientificamerican.com/article/dams-worldwide-are-at-risk-of-catastrophic-failure>
- [4] E. M. Quinn, "Dam removal: A tool for restoring riverine ecosystems," *Restoration and Reclamation Review*, vol. 5, 2000.
- [5] J. Jeon, J. Lee, D. Shin, and H. Park, "Development of dam safety management system," *Advances in Engineering Software*, vol. 40, pp. 554–563, 2009.
- [6] Federal Emergency Management Agency (FEMA). (2019) Dam failures. Accessed January 09, 2024. [Online]. Available: <https://damsafety.org/dam-failures>
- [7] C. Yu, X. Xiang, J. Zhang, R. Zhao, and C. Zhou, "Complete coverage tracking and inspection for sloping dam wall by remotely operated vehicles," in *OCEANS 2017 - Anchorage*, 2017, pp. 1–5.
- [8] A. Laidani, M. Boudria, I. Faci, A. Bouhamri, O. Kebdani, L. Rahmoun, Z. Bellahcene, and M. Bouhamida, "Design and modeling of a low-cost observation class rov for dam inspection," in *2022 2nd International Conference on Advanced Electrical Engineering, ICAEE 2022*. Institute of Electrical and Electronics Engineers Inc., 2022.
- [9] S. Shimono, S. Toyama, and U. Nishizawa, "Development of underwater inspection system for dam inspection: Results of field tests," in *OCEANS 2016 MTS/IEEE Monterey*, 2016, pp. 1–4.
- [10] X. Li, L. Li, Z. Liu, Z. Peng, S. Liu, S. Zhou, X. Chai, and K. Jiang, "Dam crack detection studies by uav based on yolo algorithm," in *2023 2nd International Conference on Robotics, Artificial Intelligence and Intelligent Control, RAIIC 2023*, 2023, pp. 104–108.
- [11] A. R. D. Mello, F. G. Barbosa, M. L. Fonseca, and C. D. Smiderle, "Concrete dam inspection with uav imagery and dcnn-based object detection," in *IST 2021 - IEEE International Conference on Imaging Systems and Techniques, Proceedings*, 2021.
- [12] C. Marín-Buzón, A. Pérez-Romero, J. L. López-Castro, I. B. Jerbania, and F. Manzano-Aguilario, "Photogrammetry as a new scientific tool in archaeology: Worldwide research trends," *Sustainability (Switzerland)*, vol. 13, 5 2021.
- [13] S. Jiang, W. Jiang, and L. Wang, "Unmanned aerial vehicle-based photogrammetric 3d mapping: A survey of techniques, applications, and challenges," *IEEE Geoscience and Remote Sensing Magazine*, vol. 10, no. 2, pp. 135–171, 2022.
- [14] X. Zhou, K. Xie, K. Huang, Y. Liu, Y. Zhou, M. Gong, and H. Huang, "Offsite aerial path planning for efficient urban scene reconstruction," *ACM Trans. Graph.*, vol. 39, no. 6, nov 2020. [Online]. Available: <https://doi.org/10.1145/3414685.3417791>
- [15] P. R. Wolf, B. A. DeWitt, and B. E. Wilkinson, *Elements of Photogrammetry with Applications in GIS*, 4th ed. New York: McGraw-Hill Education, 2014.
- [16] L. Polidori, "On laussedat's contribution to the emergence of photogrammetry," in *International Archives of the Photogrammetry, Remote Sensing and Spatial Information Sciences - ISPRS Archives*, vol. 43. International Society for Photogrammetry and Remote Sensing, 8 2020, pp. 893–899.
- [17] T. Kersten, "Digital aerial triangulation in production-experiences with block switzerland," pp. 193–204, 1999.
- [18] D. A. Palmer, "Stereoscopy and photogrammetry," *The Photogrammetric Record*, vol. 4, pp. 391–394, 4 1964.
- [19] N. Ngadiman, M. Kaamin, S. Sahat, M. Mokhtar, N. F. A. Ahmad, A. A. Kadir, and S. N. M. Razali, "Production of orthophoto map using uav photogrammetry: A case study in uthm pagoh campus," in *AIP Conference Proceedings*, vol. 2016, no. 1. AIP Publishing, 2018.
- [20] H. Eisenbeiß, "Uav photogrammetry," 2009, ph.D. Dissertation - ETH Zurich.
- [21] G. S. Avellar, G. A. Pereira, L. C. Pimenta, and P. Iscold, "Multi-uav routing for area coverage and remote sensing with minimum time," *Sensors (Switzerland)*, vol. 15, pp. 27 783–27 803, 11 2015.
- [22] K. Y. Samarakoon, G. A. Pereira, and J. N. Gross, "Impact of the trajectory on the performance of rgb-d slam executed by a uav in a subterranean environment," in *2022 International Conference on Unmanned Aircraft Systems, ICUAS 2022*. Institute of Electrical and Electronics Engineers Inc., 2022, pp. 812–820.
- [23] "Aerial Imaging: How to Achieve the Correct Ground Resolution," Available: <https://www.lumenera.com/blog/aerial-imaging-how-to-achieve-the-correct-ground-resolution>, accessed: July 22, 2023.
- [24] O. G. Ajayi, A. A. Salubi, A. F. Angbas, and M. G. Odigure, "Generation of accurate digital elevation models from uav acquired low percentage overlapping images," *International Journal of Remote Sensing*, vol. 38, no. 8–10, pp. 3113–3134, 2017.
- [25] "Blue UAS - Defense Innovation Unit," Available: <https://www.diu.mil/blue-uas>, accessed: January 15, 2024.
- [26] "Parrot Anafi USA Documentation," Available: <https://www.parrot.com/en/support/documentation/anafi-usa>, accessed: March 20, 2023.
- [27] "Parrot Olympe Documentation," Available: <https://developer.parrot.com/docs/olymp/index.html>, accessed: May 04, 2023.
- [28] A. Sarabakha and P. N. Suganthan, "anafi\_ros: from Off-the-Shelf Drones to Research Platforms," in *2023 International Conference on Unmanned Aircraft Systems (ICUAS)*, 2023, pp. 1308–1315.
- [29] D. Casini, T. Blaß, I. Lütkebohle, and B. B. Brandenburg, "Response-time analysis of ros 2 processing chains under reservation-based scheduling," in *Leibniz International Proceedings in Informatics, LIPIcs*, vol. 133. Schloss Dagstuhl- Leibniz-Zentrum fur Informatik GmbH, Dagstuhl Publishing, 7 2019.
- [30] J. L. Schönberger, E. Zheng, M. Pollefeys, and J.-M. Frahm, "Pixel-wise view selection for unstructured multi-view stereo," in *European Conference on Computer Vision (ECCV)*, 2016.
- [31] J. L. Schönberger and J.-M. Frahm, "Structure-from-motion revisited," in *Conference on Computer Vision and Pattern Recognition (CVPR)*, 2016.
- [32] W. Cornwall, "A dam big problem," *Science*, vol. 369, no. 6506, pp. 906–909, 2020. [Online]. Available: <https://www.science.org/doi/abs/10.1126/science.369.6506.906>